

# Titration Avidity of Yeast-Displayed Proteins Using a Transcriptional Regulator

Joanan Lopez-Morales, Rosario Vanella, Gordana Kovacevic, Mariana Sá Santos, and Michael A. Nash\*

Cite This: *ACS Synth. Biol.* 2023, 12, 419–431

Read Online

ACCESS |



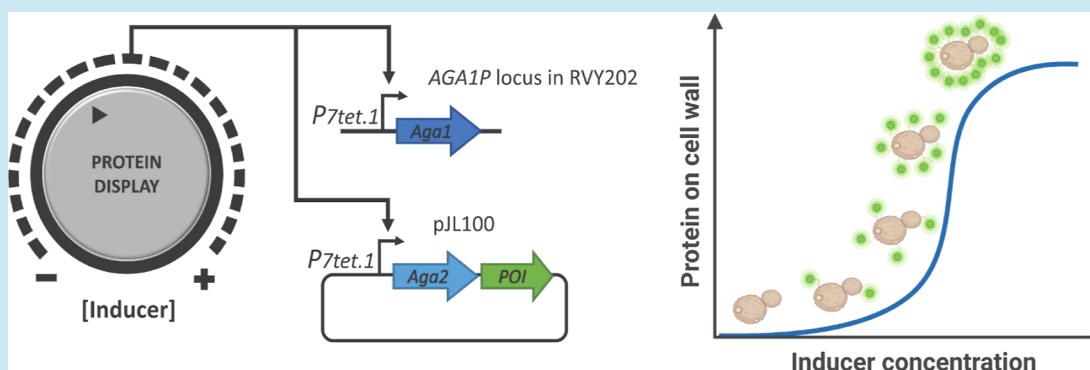
Metrics &amp; More



Article Recommendations



Supporting Information



**ABSTRACT:** Yeast surface display is a valuable tool for protein engineering and directed evolution; however, significant variability in the copy number (i.e., avidity) of displayed variants on the yeast cell wall complicates screening and selection campaigns. Here, we report an engineered titratable display platform that modulates the avidity of Aga2-fusion proteins on the yeast cell wall dependent on the concentration of the anhydrotetracycline (aTc) inducer. Our design is based on a genomic Aga1 gene copy and an episomal Aga2-fusion construct both under the control of an aTc-dependent transcriptional regulator that enables stoichiometric and titratable expression, secretion, and display of Aga2-fusion proteins. We demonstrate tunable display levels over 2–3 orders of magnitude for various model proteins, including glucose oxidase enzyme variants, mechanostable dockerin-binding domains, and anti-PDL1 affibody domains. By regulating the copy number of displayed proteins, we demonstrate the effects of titratable avidity levels on several specific phenotypic activities, including enzyme activity and cell adhesion to surfaces under shear flow. Finally, we show that titrating down the display level allows yeast-based binding affinity measurements to be performed in a regime that avoids ligand depletion effects while maintaining small sample volumes, avoiding a well-known artifact in yeast-based binding assays. The ability to titrate the multivalency of proteins on the yeast cell wall through simple inducer control will benefit protein engineering and directed evolution methodology relying on yeast display for broad classes of therapeutic and diagnostic proteins of interest.

**KEYWORDS:** titratable yeast display, directed evolution, protein engineering, synthetic biology, enzyme engineering, cell adhesion, affibody

## INTRODUCTION

Yeast surface display constitutes a core technology for *in vitro* engineering of binding proteins and enzymes.<sup>1–4</sup> Typically, yeast display is carried out in a EBY100 or a similar strain where a genomic copy of the *AGA1* gene is under the control of a galactose (GAL) promoter. Aga1 serves as an anchoring domain that binds *via* two disulfide bridges to Aga2-fusion proteins expressed from an episomal plasmid under GAL control and secreted to the cell surface. This platform allows protein evolution by screening/selecting for given phenotypes (e.g., binding or enzymatic activity), isolating pools or single cells, iterating, and ultimately recovering novel gene sequences encoding enhanced variants.

Yeast display affords proteins that have undergone eukaryotic expression and secretion. This means proteins displayed on yeast are subjected to eukaryotic post-transla-

tional quality control and modification, including glycosylation and disulfide bond formation. These features, along with the ease of genetic manipulation and stability, make yeast display a standard method for many protein engineering projects.<sup>5,6</sup> Yeast surface display has been used in the discovery and isolation of novel binders,<sup>7–14</sup> affinity maturation of antibody derivatives,<sup>15–17</sup> engineering of enzymes,<sup>18–21</sup> and enhancement of thermal,<sup>22</sup> chemical,<sup>23</sup> and mutational stability of proteins.<sup>24–26</sup> It has found further applications in kinetic and

Received: July 4, 2022

Published: February 2, 2023



competitive binding analysis,<sup>27,28</sup> protein–protein interaction studies,<sup>29–32</sup> epitope mapping,<sup>33–36</sup> and probe development for diagnostic imaging.<sup>37</sup> Recent methodological advances include coupling with combinatorial screening platforms,<sup>38</sup> introducing somatic hypermutation *in vivo*,<sup>39</sup> optimizing plasmids and cloning strategies,<sup>40</sup> continuously diversifying genes *in vivo*,<sup>39</sup> improving expression levels and protein stability,<sup>41</sup> and using diverse chemistries for conjugation and labeling.<sup>42</sup>

Despite these advances, two remaining challenges faced by current yeast surface display systems are related to expression efficiency (i.e., fraction of cells expressing the Aga2 fusion) and multivalency (i.e., protein copy number per cell).<sup>43</sup> Depending on the protein, induction under the GAL promoter can lead to widely different display levels, which can confound screening/selection campaigns for binding proteins and enzymes. Typically, immunostaining for expression levels is used for normalization;<sup>44–46</sup> however, when panning yeast libraries against cells or insoluble substrates, multivalency can strongly affect adhesion phenotypes, and depending on the workflow, normalizing for expression is not always possible. In addition to influencing binding protein behavior, multivalency can also affect enzyme engineering projects, and precisely controlling for enzyme display levels would provide significantly better control and quantification of specific activity when comparing monogenic (i.e., non-pooled) clones in head-to-head assays.

There are limited prior reports of strategies to modulate the display level of proteins on the yeast cell wall. Stern and colleagues used the disulfide reducing agent dithiothreitol to dissociate Aga1–Aga2 interactions, thereby chemically removing proteins from the surface and reducing avidity.<sup>47</sup> This approach was shown to enhance the discrimination ability for high-affinity binders but may be problematic for proteins containing disulfide bridges. Work from the synthetic biology field has demonstrated systems for titratable cytoplasmic protein production that rely on gene circuits and logic controllers to achieve transcriptional regulation.<sup>48–53</sup> For example, Azizoglu *et al.* built a well-tempered transcriptional controller (WTC<sub>846</sub>) that regulates the cytoplasmic expression of a target protein in yeast. WTC<sub>846</sub> consists of an engineered eukaryotic promoter  $P_{TDH3}$  that is repressed by the bacterial TetR repressor. Together, they comprise the enhanced  $P_{7Tet.1}$  promoter which is inducible by anhydrotetracycline (aTc). To optimize the control of genes, they added complex autorepression to the system by introducing a constitutive promoter,  $P_{RNR2}$ , which drives the expression of a second TetR gene to reduce basal expression levels. Finally, the second TetR gene was fused to the active yeast repressor Tup1 to completely eliminate basal protein synthesis. The mechanism of transcriptional control of genes by WTC<sub>846</sub>, therefore, relies on the TetR negative feedback, where TetR represses and controls its own synthesis in an aTc dose-dependent manner. The stepwise addition of aTc relieves TetR repression, leading to a tunable gradient of gene expression with a low cell-to-cell variation.<sup>54</sup>

Here, we sought to control cell phenotypic activity by titrating the copy number of proteins on the yeast cell wall. We developed a yeast titratable display (YTD) system based on the WTC<sub>846</sub> system and adapted it for the regulation and stoichiometric expression of Aga1- and Aga2-fusion proteins. We characterized and validated cell population expression efficiency and display level per cell for three model proteins [glucose oxidase (GOx), dockerin (Doc), and anti-PDL1

affibody (Affi)]. We demonstrated the capabilities of this system with three examples: (i) by normalizing and controlling the enzymatic activity of differentially active GOx variants; (ii) by quantifying and controlling the adhesion of yeasts displaying mechanostable Doc bound to surface-immobilized Cohesin (Coh) and exposed to shear stress; and finally (iii) by addressing a known artifact in yeast-based measurements of binding affinity caused by depletion of soluble ligand molecules. By limiting the copy number of anti-PDL1 affibody molecules displayed on the cell wall, we were able to quantify binding affinity correctly without scaling up reaction volumes. This titratable system, therefore, allows for quantitative measurements of binding affinity of yeast-displayed proteins while limiting reagent consumption of soluble antigens.

## METHODS

**Chemicals and Media.** Chemical reagents were purchased from Sigma-Aldrich (St. Louis, USA) unless otherwise stated. YPD medium contained 1% (w/v) yeast extract, 2% peptone (both from BD Biosciences, Germany), and 2% (w/v) glucose. Yeast Synthetic Drop-out Medium (YSD) contained 0.67% Yeast nitrogen base without amino acids (Sigma: Y0626) and 0.16% (w/v) Yeast Synthetic Drop-out Medium Supplement without leucine (YSD–Leu, Sigma: Y1376). Restriction enzymes were purchased from New England Biolabs (Ipswich, USA). aTc was acquired from Cayman Chemicals (10009542), aliquoted as 10.0 mg/mL stock in DMSO for long-term storage, and diluted in water for experiments as needed. Primary and secondary antibodies were provided by Life Technologies Corporation (Invitrogen, Massachusetts, USA). Sodium alginate (viscosity 1%:100–200 mPa·s) was purchased from Duchefa Biochemie (Haarlem, the Netherlands).

**Plasmid Cloning.** XL10-Gold Ultracompetent Cells (Stratagene, Agilent, USA) were used for plasmid preparation. Plasmids for cloning and strain engineering were kindly provided by Fabian Rudolph, ETHZ.<sup>54</sup> The plasmid for the expression of the gene of interest (GOI) pJL100 was used for titrated display. Plasmid FRP2088 carrying the  $P_{7Tet.1}$  promoter was modified with a yeast display cassette containing the fusion AGA2-epitope tags introduced by isothermal assembly. Next, the construct containing  $P_{7Tet.1}$  promoter-AGA2-epitope tags was integrated into the plasmid FRP1448 carrying a *LEU2* auxotrophic gene marker to complete the pJL100 plasmid. This vector encodes Aga2p followed by a glycine-rich peptide, a leader peptide from bacteriophage T7 gene 10, an Xpress tag, and a protease cleavage site followed by a landing pad for the GOI to be displayed, a V5 epitope, and a C-terminal Streptag epitope (Table S1). The XDocIII gene sequence in pET28a–HIS–Xyl–Xmod–DocIII (plasmid #6086<sup>55</sup>) was acquired from Addgene. The gene sequences of GOx–WT, GOx–M556L, and GOx–M556L + M561S were provided by Kovacevic.<sup>56</sup> Inserts were generated by PCR or custom DNA synthesis (Twist Biosciences, USA). GOI sequences were amplified using Phusion kits according to the manufacturer's protocol and introduced into the plasmid pJL100 by isothermal assembly. All plasmids were verified by Sanger sequencing (Microsynth AG, Switzerland) and stored at –20 °C until use. All primers and plasmids used in this work are listed in Table S1.

**Yeast Strain Engineering.** All strains described in this study derive from *Saccharomyces cerevisiae* EBY100 (background strain: BJ5465). To transform yeast, cells were grown at 30 °C in YPD medium. Transformants were isolated by

auxotrophy complementation on agar plates. For the genetic integration of constructs, plasmids were linearized with a restriction enzyme and transformed into yeast following standard lithium acetate transformation methods.<sup>57</sup> Titratable strains were generated sequentially from the parent strain RVY200, an EBY100 derived yeast strain where the *GAL1-AGA1* locus was replaced by a G418 resistance cassette through homologous recombination. The strain RVY200 carrying the plasmid for CAS9 (Nourseothricin *N*-acetyltransferase, NAT, as a marker) was co-transformed with the helper plasmid FRP2101 (Hygromycin) and a *PtetO-7.1\_Aga1* PCR construct for homology-directed repair. Positive transformants were selected on YPD + NAT + Hyg +  $\beta$ -estradiol. The *AGA1 $\Delta$ :loxp\_G418\_loxp* cassette of RVY200 was replaced with *PtetO-7.1\_Aga1* to create the RVY201 strain. Through homologous recombination in the *URA3* locus, the TetR-TUP1 controller in the linearized tagging plasmid was integrated, resulting in the final strain RVY202. Integrations were verified by PCR. Table S2 describes the genotypes of yeast strains created in this work.

**Flow Cytometry and Titrated Display Validation.** For protein display on yeast, precultures were grown overnight at 30 °C, 180 rpm in YS–Leu + 2% (w/v) glucose (Gluc) + ampicillin until saturation. The next day, the culture was diluted to OD<sub>600</sub> = 0.045 and grown at 20 °C, 180 rpm in –Leu + 2% (w/v) Gluc + ampicillin for 16 h. After the indicated growth time, the culture cell density reached an OD<sub>600</sub> = 0.4, and aTc was added at the desired concentration. To display GOx with activity on Gluc, initial cultures for dose–response analysis were grown at 30 °C, 180 rpm in YS–Leu + 2% (w/v) GAL + ampicillin medium. After 36 h, the cultures were diluted to OD<sub>600</sub> = 0.3 and further grown for 1 h at 30 °C until OD<sub>600</sub> = 0.42. The precultures were then split into 7 mL cultures, and aTc was added at the corresponding concentration for protein expression.

For expression profiles without dose response over time, protein expression and display were induced for 5 h. For aTc dose responses, cultures were sampled every hour for 8 h, where 5 million cells were taken and washed with PBS + 0.1% BSA. Protein translation was stopped after the desired induction time by adding Cycloheximide (Sigma: 239765-1ML) at 200 ng/mL. Displayed proteins in the cell pellets were labeled at the C terminus using a primary mouse anti-V5 (E10/V4RR) monoclonal IgG antibody (1:500, Cat: MA5-1523) and a secondary goat anti-mouse IgG (H + L) Highly Cross-Adsorbed antibody conjugated to AlexaFluor 594 dye (1:500, Cat: A-11032).

Cytometric analyses were done on an Attune NxT flow cytometer (Thermo Scientific, USA) equipped with a high-throughput autosampler and 488 and 561 nm lasers. The fraction of cells displaying the protein of interest (POI) was obtained by gating out the uninduced population. The relative protein amount per cell was observed as the median fluorescence of the analyzed population. GOx activity was verified by flow cytometry using single-cell encapsulation of displaying cells in alginate hydrogel microspheres, as previously described.<sup>21</sup>

**GOx Activity Assay in a Cell-Based Format.** Cultures of each GOx variant were grown in YS–Leu–Gal medium and induced for 5 h at different aTc concentrations.  $4 \times 10^6$  cells were washed with PBS + 0.1% BSA, immunolabeled as described before, and checked for full-length GOx display by flow cytometry. 500,000 unlabeled cells underwent a GOx

activity test, as described previously.<sup>58</sup> Briefly, 100 mM glucose, 4  $\mu$ M horseradish peroxidase (HRP), and 1.83 mM ABTS (2,2'-azino-bis(3-ethylbenzothiazoline-6-sulfonic acid)) were mixed in 200  $\mu$ L of filtered PBS and added to the respective cell suspension in triplicates. GOx activity was measured by absorbance at 405 nm on a TECAN plate reader in continuous mode for 10 min. Relative activity slopes were normalized ( $n = 3$ ).

**Adhesion Assay.** An in-house device based on a spinning disk cell adhesion assay was employed to study cell population adhesion profiles. The construction of the apparatus and coverglasses' preparation were performed as described previously.<sup>59,60</sup> Briefly, aminosilanized coverglasses were functionalized with Cohesin E (CohE–HIS–ybbR) using a 250  $\mu$ M solution of Maleimide–PEG–NHS (5 kDa; Rapp Polymere, Tübingen, Germany) in 25 mM CH<sub>3</sub>O–PEG–NHS (5 kDa; Rapp Polymere, Tübingen, Germany) and 100 mM HEPES pH 8 for 30 min. Coverglasses were rinsed with ultrapure water and incubated with 200  $\mu$ M Coenzyme A (CoA) solution for 30 min. After washing with ultrapure water, CoA coverglasses were incubated with the CohE–HIS–ybbR fusion protein in 5  $\mu$ M 4'-phosphopantetheinyl transferase Sfp, 10 mM MgCl<sub>2</sub>, and TBS–Ca<sup>2+</sup> pH 7.4 buffer for 30 min. Then, the surfaces were rinsed with ultrapure water and immediately blocked with 5% BSA in PBS for 30 min.

Yeast cell populations displaying Aga2–Doc (specifically, XDocIII from *Ruminococcus flavefaciens*<sup>55</sup>) after induction for 4 h at variable aTc concentration were seeded and allowed to adhere to the coverglasses for 30 min. The cell suspension was removed from the adhesion assay by gentle pipetting with a syringe and replaced with TBS–Ca<sup>2+</sup>. The cells on the disk underwent a spinning program consisting of a 20 s acceleration ramp, a 5 min constant spinning at the indicated angular velocity (rpm), and a 20 s deceleration in a TBS–Ca<sup>2+</sup> buffer chamber. Image analysis and data treatment were performed as described elsewhere.<sup>59</sup> Detachment profiles for  $n = 3$  technical replicates were plotted and fitted using a global sigmoid probabilistic model to extract the shear stress value ( $\tau_{50}$ ), at which 50% of the cells remained adherent.<sup>61</sup> The  $\tau_{50}$  value was used as a measure of the mean adhesion strength for comparison of the different cell populations.

**Binding Assays by Flow Cytometry.** For the standard yeast display using a pYD1 plasmid and GAL promoter, cultures of anti-PDL1 affibody were grown overnight at 30 °C, 180 rpm in YS–Trp + 2% Gluc + ampicillin medium, and then they were transferred to YS–Trp + 1.8% (w/v) Gal + 0.2% (w/v) Gluc + ampicillin medium pH 5.0 at 20 °C, 180 rpm. The anti-PDL1 affibody display was induced for 48 h.  $2 \times 10^6$  cells were washed with PBS + 0.1% BSA, immunolabeled as described before, and checked for full-length affibody display by flow cytometry. For binding experiments using the GAL yeast display,  $5 \times 10^5$  cells were washed, pelleted, and then resuspended in serial dilutions of biotinylated human PDL1 in PBS + 0.1% BSA for 3 h at 20 °C.

In the case of the correct assessment of the anti-PDL1 affibody's apparent binding affinity ( $K_D$ ), the labeling volume must be large enough to allow yeasts to stay in suspension and should be chosen such that ligand binding to yeast-displayed anti-PDL1 affibody is not under depleting conditions. Therefore, the volume was increased accordingly for lower ligand concentrations to maintain a ligand excess of at least 10-fold over the anti-PDL1 affibody displayed on  $5 \times 10^5$  cells.

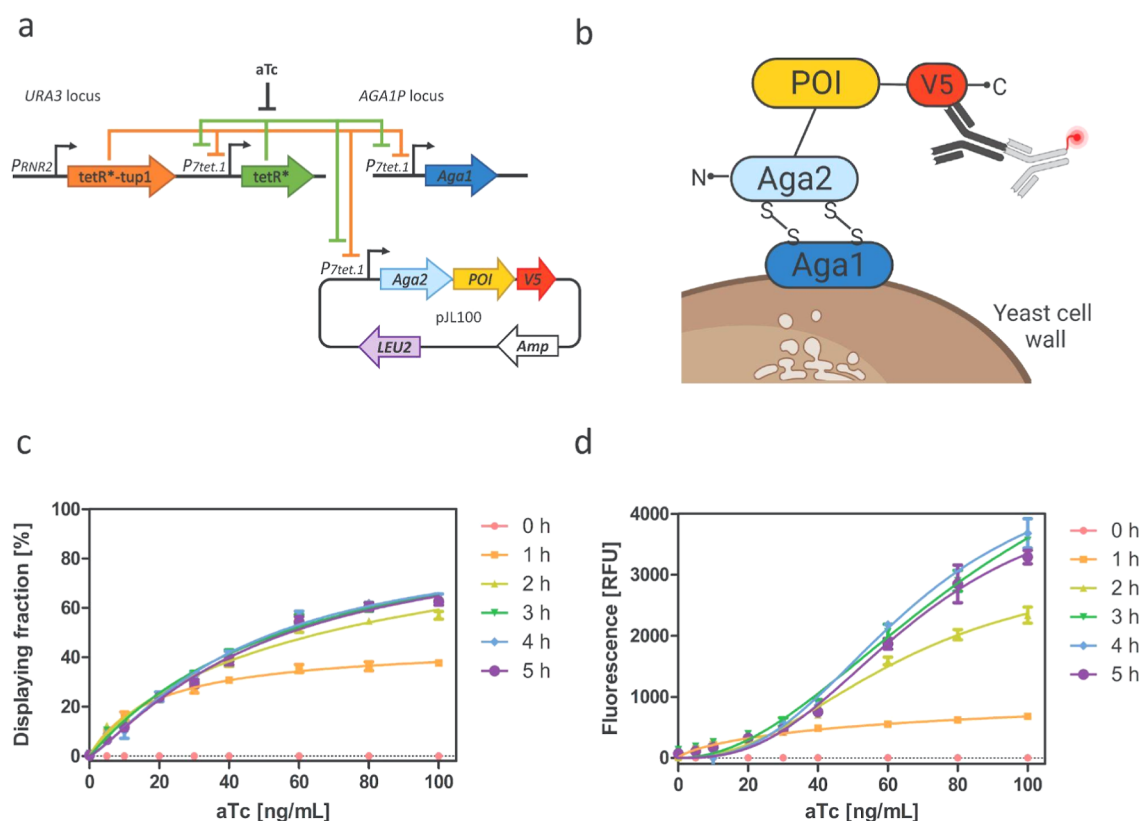


**Figure 1.** Architecture and characterization of the YTD system. (a) The YTD system comprises two integrative constructs, TetR and TetR–Tup1, regulated by the  $P_{7tet.1}$  and  $P_{RNR2}$  promoters,<sup>54</sup> respectively. The \* symbol represents an SV40 nuclear localization sequence. The  $P_{7tet.1}$  promoter acts on both Aga1 and Aga2 proteins simultaneously to deliver a stoichiometric and titrated display of the POI. The final strain containing the integrated YTD is RVY202, which works with an episomal pJL100 plasmid harboring the GOI fused to Aga2 under  $P_{7tet.1}$  control. (b) Overview of the YTD cell surface. The displayed construct is identical to a standard Aga1–Aga2 yeast display system and can be readily immunolabeled. (c) Fraction of cells displaying a POI (Aga2–V5 tag) as a function of time and inducer concentration. (d) The amount of displayed POI per cell (median fluorescence of Aga2–V5 tag). Error bars represent the standard deviation of the mean ( $n = 3$ ). RFU: relative fluorescence units.

The anti-PDL1 affibody concentration [Affi] (in nanomolar) in the sample was calculated as follows

$$[\text{Affi}] = \frac{\delta \cdot N_{\text{cells}} \cdot f_{\text{Disp}} \cdot 1 \times 10^{12}}{N_A \cdot V_{\text{Rxn}}}$$

where  $\delta$  is the number of displayed molecules per cell taken as  $5 \times 10^4$  molecule per cell,<sup>62</sup>  $N_{\text{cells}}$  is the number of cells in the reaction volume ( $5 \times 10^5$  cells),  $f_{\text{Disp}}$  is the displaying fraction of cells in the sample,  $N_A$  is Avogadro's number  $6.022 \times 10^{23}$  molecules·mol<sup>-1</sup>, and  $V_{\text{Rxn}}$  is the final volume of the binding reaction at a specific ligand concentration, mL. For the ligand depletion effect demonstration,  $5 \times 10^5$  cells were washed, pelleted, and resuspended in serial dilutions of biotinylated human PDL1 in PBS + 0.1% BSA for 3 h at 20 °C in a fixed volume of 0.05 mL of ligand dilutions.

In the case of the YTD system, cultures of anti-PDL1 affibody were treated as previously described, except that the medium was buffered with 0.1 M phosphate-citrate buffer pH 5.0. The affibody display was induced for 4 h at different aTc concentrations. For binding experiments,  $5 \times 10^5$  cells were washed, pelleted, and then resuspended in serial dilutions of biotinylated human PDL1 in PBS + 0.1% BSA for 3 h at 20 °C in a fixed volume of 0.05 mL of ligand dilutions.

After incubation, the cells were rinsed with 1 mL of ice-cold PBS + 0.1% BSA and labeled for flow cytometry analysis. All the following steps were done at 4 °C. Briefly, washed cells

were incubated in 100  $\mu$ L of Neutravidin-FITC 1:50 dilution + primary mouse anti-V5 mAb (1:500) in PBS + 0.1% BSA for 25 min at 4 °C. Pelleted cells were washed with 1 mL of ice-cold PBS + 0.1% BSA and labeled with a secondary goat anti-mouse mAb conjugated to AlexaFluor 594 dye (1:500) for 20 min at 4 °C. Cells were washed with 1 mL of ice-cold PBS + 0.1% BSA and resuspended in 0.5 mL of PBS + 0.1% BSA only before flow cytometry.

The apparent affinity of the anti-PDL1 affibody was calculated by drawing a gate that excluded the non-displaying fraction of cells and quantifying the mean fluorescence intensity from the FITC channel of the displaying fraction (MFU<sub>tot</sub>). To plot the fraction bound  $Y$ , normalization was performed by subtracting the mean fluorescence of the zero-ligand sample ( $[\text{PDL1}] = 0$  nM, MFU<sub>min</sub>) from the MFU<sub>tot</sub> of each point and then dividing by the mean fluorescence of the lowest ligand dilution ( $[\text{PDL1}] = 1$   $\mu$ M, MFU<sub>max</sub>), all versus ligand concentration ( $[\text{PDL1}]$ ). The data fit the following equation

$$Y = \frac{\text{MFU}_{\text{max}} \cdot [\text{PDL1}]}{[\text{PDL1}] + K_D}$$

$[\text{PDL1}]$  was assumed to be constant as it is in large excess relative to the [Affi] and therefore is approximately equal to the initial  $[\text{PDL1}]$  concentration. The data from  $n = 2$  independent experiments were plotted, and the sum of the square of the differences between the measured and predicted

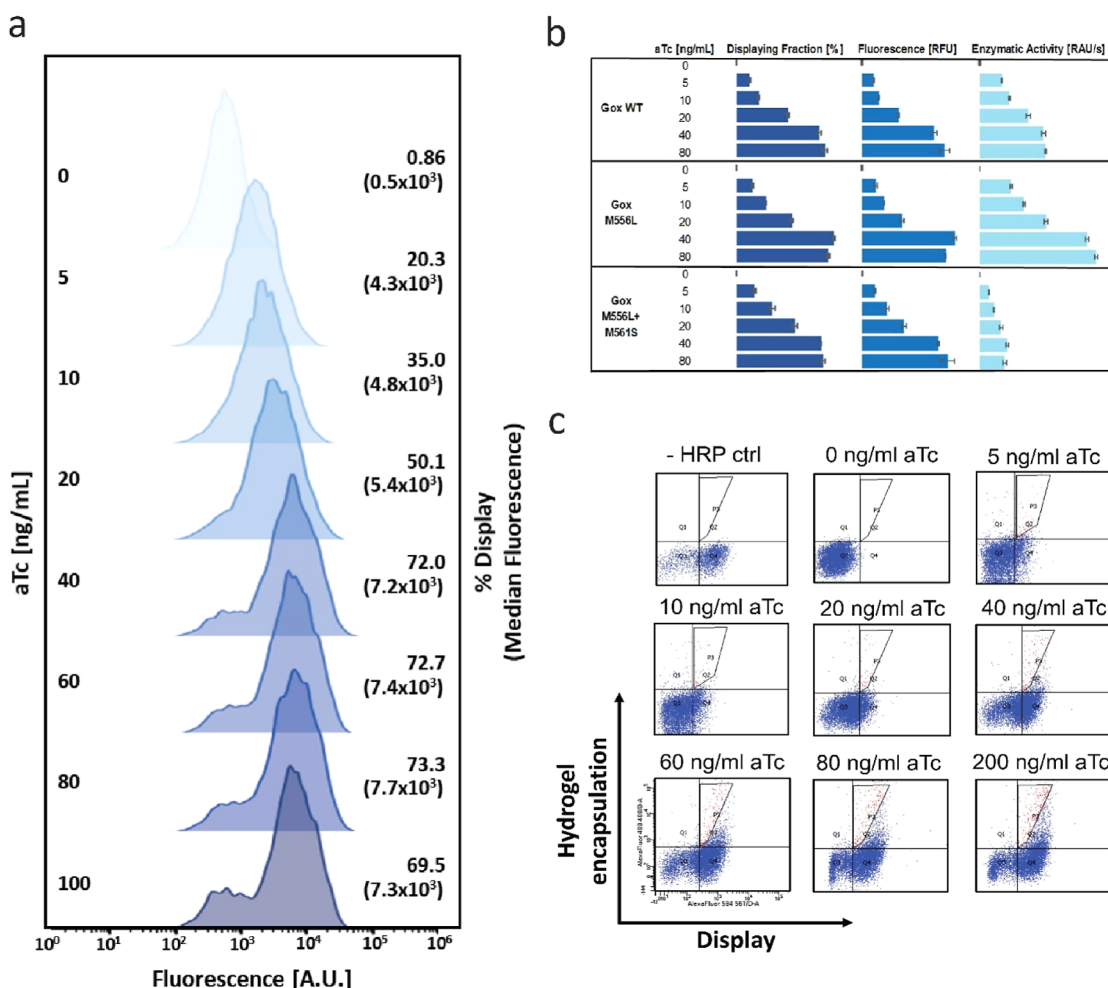


**Figure 2.** Titrated display and enzymatic activity of dimeric GOx variants. (a) Display-level histograms for dimeric GOx–WT in the YTD system with 15,000 cells analyzed per histogram. The median fluorescence of the displaying population is shown in brackets. (b) YTD was used to titrate the displaying fraction of cells (%) and the amount of displayed enzyme per cell [fluorescence (RFU)]. Enzymatic activity for each culture at fixed cell numbers was measured using a colorimetric assay. Error bars represent the standard error of the mean ( $n = 3$ ). (c) Titration of hydrogel encapsulation of single cells displaying pooled GOx variants;  $n = 1$  M single cells; the triangular gate encloses the fraction of encapsulated cells.

values based on the fitted equation was used as the loss function to minimize the error as a function of the two free parameters ( $K_D$  and  $MFU_{max}$ ). The apparent  $K_D$  was determined using GraphPad's Prism non-linear fitting tool for the one site-specific binding model.

## RESULTS AND DISCUSSION

### Construction and Characterization of a YTD System.

To develop our YTD system for titrating the avidity of yeast-displayed proteins, we employed the previously reported transcriptional well-tempered controller<sub>846</sub> (WTC<sub>846</sub>)<sup>54</sup> and adapted it to regulate display levels of Aga1- and Aga2-fusion proteins in response to aTc in a dose-dependent manner. We hypothesized that by placing both the Aga1 anchor and the Aga2–POI fusion under the control of WTC<sub>846</sub>, our YTD system could enable stoichiometric expression of both components required for standard yeast display and allow titratable display of the POI from an episomal plasmid (Figure 1a). The final YTD design consists of the engineered RVY202 strain and the carrier vector pJL100. To regulate protein expression and display, we constructed the yeast strain RVY200 where we substituted the GAL promoter with the  $P_{7Tet.1}$  promoter upstream of the genomic AGA1 copy and

introduced the repressor *TetR-nls-Tup1* fusion into the *URA3* locus. The complementary AGA2 for yeast surface display was built as an episomal copy where the  $P_{7Tet.1}$  promoter was introduced upstream of a yeast display cassette containing standard AGA2-terminal tags (Xpress + V5). The fusion was then transferred to a plasmid carrying a *LEU2* auxotrophic gene marker to complete the pJL100 plasmid. The protein elements of the display cassette remain identical to those used in standard yeast surface display, and the titration is achieved by the  $P_{7Tet.1}$  promoter upstream of the AGA2 fusion (Figure 1b).

Following the construction of the strain and plasmid, we assessed the range of display levels at different aTc concentrations by inducing the empty cassette containing Aga2 followed by Xpress and V5 tags and staining for the V5 tag. Flow cytometric analysis showed that the YTD system effectively modulated the fraction of cells displaying the POI (5–10% with 10 ng/mL aTc, 20–30% with 20 ng/mL aTc, 40–50% on 40 ng/mL aTc and reaching a saturated display of >60% with >60 ng/mL aTc up to a maximum dose of 200 ng/mL aTc). Simultaneously, the amount of POI displayed per cell was titrated in response to a range of inducer concentrations from 0 to 200 ng/mL aTc [ $<1000$  relative

fluorescence units (RFU) with 10–20 ng/mL aTc, 1000–2000 RFU with 40–60 ng/mL aTc, 2000–3000 RFU with 60–80 ng/mL aTc, and above 4000 RFU with >80 ng/mL aTc]. The plateau of the median fluorescence for an empty cassette set in at 100 ng/mL aTc. For larger constructs, the plateau set in at lower aTc concentrations (~60 ng/mL). The number of molecules per cell at saturation was typically 10-fold lower than standard yeast display with the GAL inducer (Table S3). ATc concentrations >60 ng/mL resulted in a saturation of both the percentage of cells displaying the POI (~60–90% depending on the construct) and the amount of displayed POI per cell (4000 to >6000 RFU depending on the construct). The YTD system reached maximum display levels 5 h after aTc induction, significantly shorter than the GAL-induction system, which generally requires an average of 24–36 h, up to 48 h for reaching saturation of display levels<sup>1</sup> (Figures 1c,d and S1).

**Titration Enzymatic Activity on the Yeast Cell Surface.** We next tested whether YTD could regulate enzyme copy number on the cell wall and influence the resulting specific activity. To do so, we inserted GOx as the POI in our YTD system. GOx is a homodimeric enzyme that oxidizes  $\beta$ -D-glucose to D-gluconolactone and hydrogen peroxide.<sup>64</sup> Prior work by Kovacevic and colleagues showed that the single-mutant GOx-M556L and the double-mutant GOx-M556L + M561S exhibit enzymatic activities above and below (respectively) GOx-WT at pH 5.5.<sup>56</sup> We employed these two mutants along with the WT-GOx sequence as a model set of variants with known catalytic activities. We titrated the display levels of dimeric full-length GOx-WT and the two mutants (GOx-M556L and GOx-M556L + M561S) using 5 h of induction over a range of aTc concentrations. During the GOx induction, GAL was used as the carbon source to avoid premature generation of peroxide and toxic effects on the cells during expression.

Fluorescence-activated cell sorting (FACS) analysis was then conducted to assess the fraction of cells positively induced for GOx expression. Figure 2 shows flow cytometric and GOx activity assay results of the three variants. Both GOx mutants and WT were successfully displayed and titrated by aTc over a range from 0 to 80 ng/mL. An increase in the fraction of cells displaying GOx-WT and the amount of displayed GOx-WT per cell (median fluorescence) confirmed the modulation of enzyme display levels (Figure 2a).

We measured the total observable enzymatic turnover from different GOx-displaying yeast cultures (GOx-WT, GOx-M556L, and GOx-M556L + M561S) (Figure 2b). We found that the fraction of cells displaying the respective GOx variants and their median fluorescence per cell were all similar. At the same time, there were significant differences in their enzymatic activities. At the maximal inducer concentrations (80 ng/mL aTc), cells displaying GOx-WT remained as the middle reference with a turnover measured at  $20.0 \pm 0.2 \text{ A.U.} \times 10^{-3} \text{ s}^{-1}$ . Meanwhile, cells expressing the more active GOx-M556L exhibited a turnover of  $35.0 \pm 0.5 \text{ A.U.} \times 10^{-3} \text{ s}^{-1}$ . The culture displaying the double-mutant GOx-M556L + M561S had the lowest activity of  $8.0 \pm 0.6 \text{ A.U.} \times 10^{-3} \text{ s}^{-1}$ . All activity measurements were made at a fixed cell suspension concentration of  $2.5 \times 10^6$  cells/mL. These activity levels were consistent with the catalytic behaviors previously reported by Kovacevic and colleagues for the GOx-M556L variant. For the double-mutant GOx-M556L-M561S, prior characterization at pH 5.5 indicated similar or slightly increased activity compared to WT, while here all enzymes were assayed at pH 7.4. Given

that the amount of enzyme (median fluorescence) on the cell wall was similar for all variants (Supporting Table S4), we attributed the observed differences to differences in the catalytic activity of the variants under the assay conditions used here. We found that GOx-M556L reached the same activity level at 20 ng/mL aTc as the GOx-WT culture at 80 ng/mL aTc. Similarly, GOx-M556L at 5 ng/mL aTc reached a similar or slightly higher turnover as the lower performing GOx-M556L + M561S achieved at maximal induction.

We next tested the titration of GOx enzymatic activity using a hydrogel-based readout that we previously developed as a high-throughput method.<sup>65</sup> In this system, chemically modified alginate is crosslinked by the GOx/HRP cascade, thereby encapsulating single yeast cells in hydrogel shells in response to displayed GOx activity. We found that the extent of encapsulation of the yeast cells in fluorescent hydrogel capsules could be straightforwardly controlled using YTD under different inducer concentrations (Figure 2c), mirroring the observations from the microwell-based turnover assays. These results directly correlate with the amount of enzyme per cell (median fluorescence) as a function of aTc. While working with enzyme libraries with heterogeneous expression of variants would still require normalization to reduce bias, the YTD system can serve as a tool for developing quantitative screening methods for enzymes based on activity control and regulation of enzyme density per cell. The YTD system, therefore, offers a means to regulate enzyme expression levels as an additional tunable parameter in the development of quantitative enzyme assays for comparison of variants.

#### Titration Cell Adhesion Strength under Shear Stress.

Next, we studied the effects of titrating surface receptors on the adhesiveness of yeast cell populations under exposure to shear stress. Since adhesion to surfaces under hydrodynamic flow is a process that is highly dependent on multivalency, we sought to demonstrate tuning of adhesiveness based on the titration of displayed receptors. We used the interaction between Coh and Doc from *R. flavefaciens* as a model cell adhesion complex. The CttA X-module dockerin III (XDocIII) is a 54 kDa domain that tightly binds its cognate Cohesin E (CohE). Both proteins serve as anchor units in a supramolecular structure called the cellulosome, a multi-scaffold complex assembled on the cell wall of various anaerobes that adheres to and digests cellulose substrates.<sup>55,66,67</sup> The interaction between XDocIII and CohE is mechanically very strong, and we hypothesized that it would proportionally mediate cell adhesion strength when titrated with the YTD system.

We inserted XDocIII as the POI into the YTD system, titrated its display level on the yeast cell surface, and measured the resulting cell adhesion strength. We used a surface covalently modified with a fixed density of the binding partner CohE and performed a spinning disk assay (SDA) to quantify the adhesion strength. In the SDA, cells are adhered onto a ligand-functionalized coverglass and undergo a spinning procedure that generates a gradient of hydrodynamic shear stress to remove cells. The shear stress at which 50% of the cells are observed to detach ( $\tau_{50}$ ) can be used to quantify the average cell adhesion strength for the cell population.<sup>60,61,68,69</sup>

In our implementation of the SDA, yeast adhesion is mediated primarily by the displayed POI and should therefore be strongly influenced by protein levels at the cell surface. The display level was titrated with different aTc concentrations for 4 h of induction, and analytic flow cytometry was performed to verify successful titration of the fraction of cells displaying

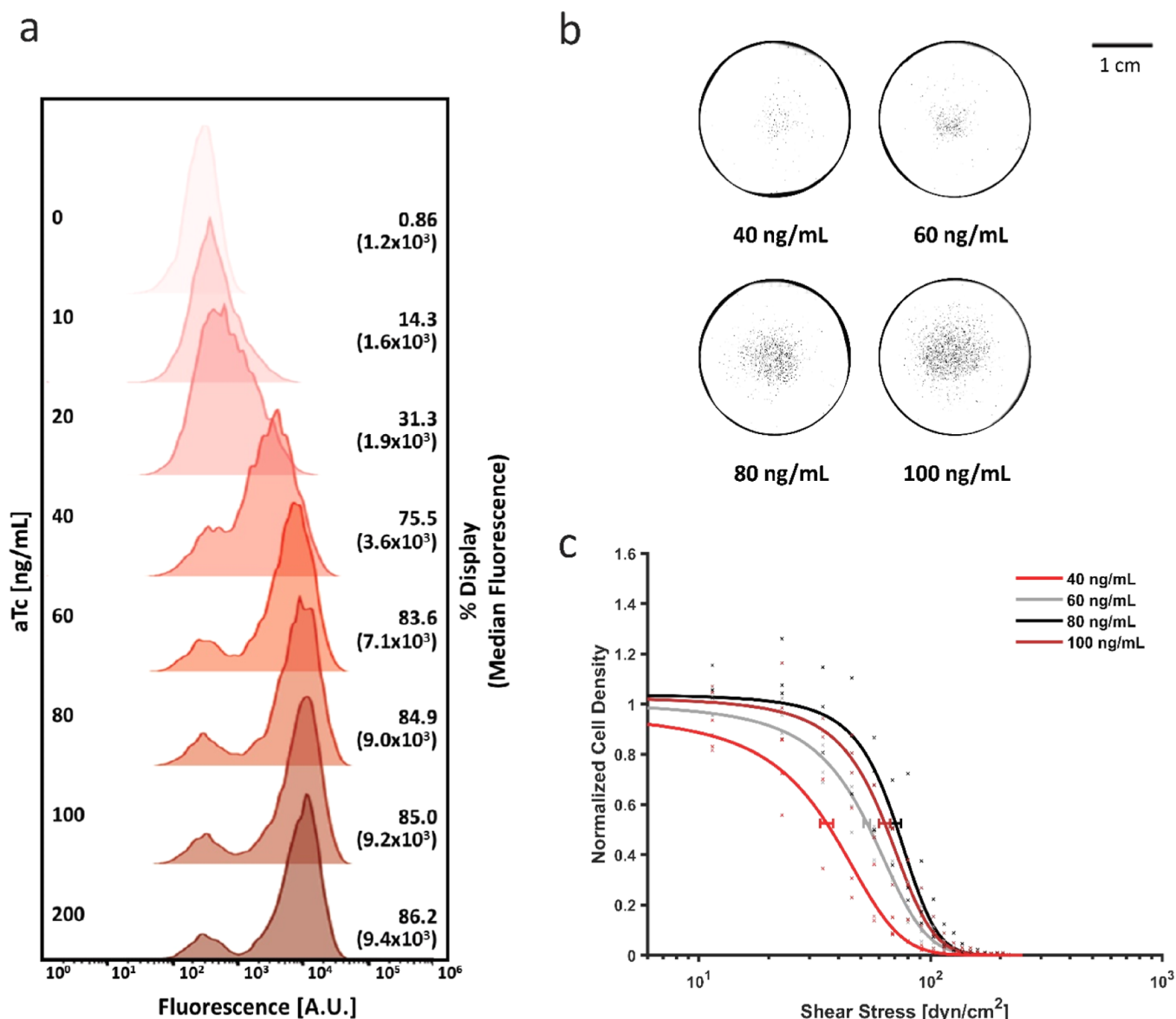


**Figure 3.** Titrated adhesion strength under shear flow. (a) Histograms showing displayed XDocIII levels for various aTc inducer concentrations (0–200 ng/mL inducer; 10,000 cells per histogram). The median fluorescence of the displaying population is shown in brackets. (b) Images of CohE-modified coverglasses with adhered yeast cells displaying titrated levels of XDocIII after exposure to hydrodynamic shear stress. Yeast cells were marked as black dots by image processing software. (c) Inducer-dependent detachment profiles of cells displaying XDocIII ( $n = 3$  for each line). Solid lines show the global fits to a sigmoid model, which determines the shear stress value at which 50% of cells are detached.

XDocIII and the amount of displayed protein per cell. Figure 3a shows an increase in the fraction of displaying cells induced in the range of 0–200 ng/mL of aTc, as well as the corresponding median fluorescence per cell, confirming the successful titration of XDocIII. Yeast populations displaying XDocIII at different levels were allowed to settle onto CohE-functionalized coverglasses and then spun at 2000 rpm to generate adhesion profiles. Subsequently, the coverglasses were imaged, and the cell density of the adherent population was calculated in concentric sections of the disk. Cell density values were normalized to the density at the center of the disk, where the shear stress was zero. We found that indeed the protein level at the cell surface was correlated with the cell density after the spin, indicating resistance to higher shear stress (Figure 3b) for cells displaying higher copy numbers of receptors. This trend resulted in a rightward shift of the adhesion profile for XDocIII cells with the increase in aTc concentration used

during induction (Figure 3c). The adhesion strength ( $\tau_{50}$ ) of each population was extracted from a global fit of three technical replicates, yielding values of  $35.62 \pm 2.28 \text{ dyn} \cdot \text{cm}^{-2}$  for cells induced with 40 ng/mL aTc,  $53.18 \pm 1.72 \text{ dyn} \cdot \text{cm}^{-2}$  for 60 ng/mL aTc,  $70.61 \pm 3.68 \text{ dyn} \cdot \text{cm}^{-2}$  for 80 ng/mL aTc, and  $63.47 \pm 3.56 \text{ dyn} \cdot \text{cm}^{-2}$  for 100 ng/mL aTc. As in the previous dose–response experiments with the YTD, a dose of >60 ng/mL aTc saturated the displaying cell fraction and median fluorescence with no further increase in adhesiveness at higher inducer concentrations. These data demonstrate how the adhesiveness of the cells under shear stress follows the display-level titrated by the YTD, where maximum adhesion was achieved after reaching the maximum display level at 5 h post aTc induction for aTc >60 ng/mL.

Furthermore, the adhesion strength measured by the fitted  $\tau_{50}$  values was correlated linearly with the median fluorescence per cell and, therefore, to the amount of XDocIII on the cell

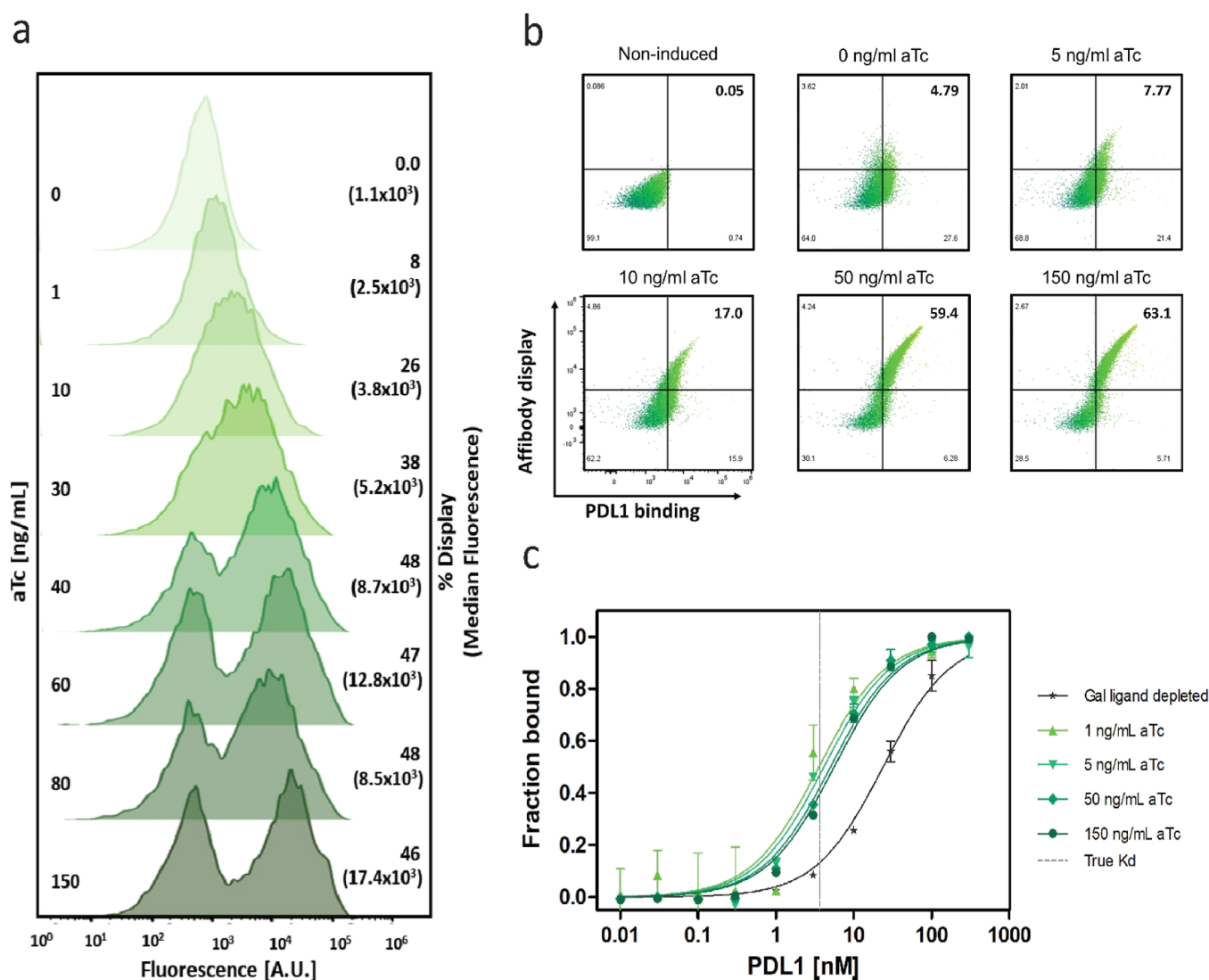


**Figure 4.** Titrated display of anti-PDL1 affibody and correction of ligand-depletion effect in low-volume immunoassay. (a) Inducer-response histograms of 15,000 single cells displaying anti-PDL1 affibodies induced over a range of aTc concentrations from 0 to 200 ng/mL. The fractions of cells displaying affibodies are shown as percentages to the right of the corresponding histogram. The median fluorescence of the displaying population is shown in brackets. (b) Titrated binding of displayed anti-PDL1 affibodies to PDL1. Two million cells induced with different concentrations of aTc were incubated with 300 nM PDL1-FITC. An increase in bound cells as a function of aTc concentration was observed by flow cytometry. Enlarged bold numbers in quadrant 2 represent the displaying fraction of cells binding to PDL1 (percentage). (c) Correction of ligand depletion artifacts by displaying anti-PDL1 affibody at low levels and comparison with a standard GAL-induced yeast display system. The YTD allows the correct calculation of the affinity constant ( $K_D$ ) in small volumes, while the standard system suffers from depletion effects under the same reaction conditions. Data fitting and affinity constant calculations were performed in GraphPad Prism, employing a model for single-site binding.

wall (Figure S2). Avidity reduction using the YTD system decreased the number of XDocIII receptors that were able to bind to the CohE-modified coverglass, thereby lowering the shear stress that could be withstood by the cell population. We noted that the mechanical response of molecular adhesion bonds will vary greatly depending on the tether positions used to fix the binding partners to the yeast and the surface. In our case, XDocIII is attached through its N terminus to the Aga2 anchor, which mimics its natural configuration. The titration of the protein on the cell wall directly influences the total number of bonds under shear stress and, consequently, the adhesion profiles. These data demonstrate the potential of the YTD for titration of yeast cells' adhesion to solid surfaces or surface-immobilized ligands, facilitating the study and normalization of display-dependent binding under shear forces.

### Titrating Non-Antibody Scaffolds for Low-Volume Yeast-Based Immunoassays.

To demonstrate the effects of titratable multivalency on soluble antigen binding, we titrated the display of a high-affinity mini protein called affibody. The affibody we used was evolved to bind to human programmed death ligand-1 (i.e., anti-PDL1 affibody<sup>70,71</sup>). We introduced the gene encoding the anti-PDL1 affibody as the POI into the YTD system and induced it for 4 h over the aTc range from 0 to 150 ng/mL. As in the previous examples, we found that the YTD system successfully modulated the percentage of displaying cells as well as the number of affibody molecules per cell. In the case of small proteins like affibody (6 kDa) or single-domain antibodies (12–15 kDa), we observed that the range of inducer that could modulate display levels was wider, extending to 150 ng/mL (Figure 4a), which was higher than

for larger and more complex proteins [e.g., XDocIII (~26 kDa) and GOx (160 kDa dimer)], which were saturated at <60 ng/mL aTc. Yeast cells displaying anti-PDL1 affibodies showed strong binding to PDL1, indicating functional expression and folding of affibody as an Aga2 fusion on the cell wall. The number of affibodies on the cell surface directly correlated with the inducer concentration and demonstrated titrated binding to PDL1 on FACS (Figure 4b).

We hypothesized that the ability of the YTD system to reduce the number of displayed molecules per cell could be advantageous in addressing a well-known artifact in heterogeneous immunoassays called the ligand depletion effect.<sup>63,72–78</sup> This experimental artifact leads to the significant overestimation of the equilibrium dissociation constant ( $K_D$ ) when the soluble ligand is not kept in large excess to the number of surface-binding sites on the yeast (or other heterogeneous immunoassay surfaces). The depletion of the soluble ligand leads to a regime where the approximation of the constant total free receptor and free ligand is no longer valid, leading to a right shift of the binding curves and an apparent  $K_D$  value that is larger than the true value. Theoretically, this effect could be avoided by simply decreasing the number of cells in the assay volume; however, from a practical standpoint, a minimum number of yeast cells (~500,000) is required to successfully pellet the cell suspension to remove/wash unbound ligand molecules. To overcome this issue, published protocols recommend scaling up the solution volume at low ligand concentrations but this has the disadvantage that large quantities of the soluble ligand are required. For ultra-high-affinity binding interactions where the ligand must be titrated to very dilute concentrations (<low nM), required assay volumes can be very large (>10 mL) to maintain the assay in a range where the ligand depletion artifact is avoided. To overcome this limitation, we show below how the YTD can be used to titrate down the display levels and maintain assay conditions that avoid ligand depletion effects even while keeping the reaction volume very small (~100  $\mu$ L) and the number of yeast cells in a range where they can still be pelleted and washed with standard lab equipment.

In practice, it is customary to keep the concentration of the antibody below the  $K_D$  for the binding reaction. For our system, this means keeping the total affibody concentration much less than  $K_D$  ( $[Affi]_{total} \ll K_D$ ). When this condition is true at all concentrations of PDL1, the amount of PDL1 in the Affi-PDL1 complex is only a negligible fraction of the  $[PDL1]_{Total}$  and the ligand depletion effect is negligible and free  $[PDL1]$  approximates  $[PDL1]_{total}$  ( $[PDL1] \approx [PDL1]_{total}$ ). This condition is useful because free  $[PDL1]$  is not easily measured, and a simplified approximate binding model equation can be employed

$$\frac{[Affi-PDL1]}{[Affi]_{total}} \approx \frac{[PDL1]_{total}}{[PDL1]_{total} + K_D}$$

First, we determined the  $K_D$  of the affibody–PDL1 interaction using conventional yeast display of affibody under the control of the GAL promoter. This was done by fixing the total number of affibody-displaying yeast cells in a fixed volume (i.e., 500,000 cells), while soluble PDL1 was added over a range of concentrations. From this analysis, we obtained  $K_D = 3.659 \pm 0.2338$  nM (Figure S3), where the reaction volumes of the high-dilution PDL1 samples were very large (>1 mL at 1–

3 nM PDL1, >10 mL at 0.1–0.3 nM PDL1, and >40 mL at <0.03 nM PDL1).

Using this  $K_D$  value as a starting point, we performed numerical calculations to simulate the binding curves and observe the ligand depletion effect. To simulate the binding curves under the first condition ( $[Affi]_{total} \ll K_D$ ), we used a tabular method (initial, change, equilibrium reaction table), where the total (or initial) molarities  $[Affi]_{total}$  and  $[PDL1]_{total}$  were introduced as the initial values. Assuming a  $K_D = 3.65$  nM, an average number of  $5 \times 10^4$  molecules displayed per cell, 0.5 million cells as the minimum number of yeast cells that can be easily pelleted, and a binding reaction volume of 0.1 mL, free  $[Affi]$  and free  $[PDL1]$  at equilibrium were calculated for every  $[PDL1]_{total}$  reaction condition. Simulated binding curves were constructed by calculating the fraction of bound affibody on the yeast surface  $[Affi-PDL1]/[Affi]_{total}$ . The calculation was repeated for each PDL1 ligand dilution over a range of cell numbers per reaction volume. As the number of cells changes, the  $[Affi]_{total}$  changes accordingly. The fraction bound was plotted against the  $[PDL1]_{free}$  and fitted to obtain true binding curves (Figure S4a). The  $K_D$  obtained from fitting these curves is in perfect accordance with the input  $K_D$ . However, this idealized binding curve cannot be obtained straightforwardly from experimental data because the  $[PDL1]_{free}$  is not readily measurable in the yeast-based immunoassay.

If the binding curves are calculated using the approximation that  $[PDL1]_{free} \approx [PDL1]_{total}$ , the accuracy of the  $K_D$  estimation is severely affected by ligand depletion effects under specific circumstances. Experimentally, ligand depletion can occur when  $[Affi]_{total} \gg K_D$ , either because too many cells were used for the measurement or because the volume of the binding reaction was not adjusted to keep the  $[PDL1]_{total}$  in large excess over the  $[Affi]_{total}$ . Both situations were simulated and depicted in Figure S4b,c, respectively. If the yeast samples were processed in fixed volumes of 0.1 mL and the number of cells changes, then the obtained  $K_D$  deviates from the original value of  $K_D = 3.65$  nM. Using less than 0.1 million cells for this fixed volume would be necessary to get a better-approximated  $K_D$ ; however, this is below the minimum number that can be pelleted and washed. Given that 0.5 million cells are a reasonable number of cells to pellet and wash, a minimal volume of 30 mL is required to obtain  $K_D$  with better accuracy and avoid ligand depletion effects.

The simulations describe routine considerations that must be accounted for when working with the standard yeast display.<sup>77</sup> The main restrictions of this system are the limits for the minimal numbers of cells that can be precisely manipulated and the titration level of affibody binders on the yeast surface. For ultra-high-affinity binding interactions, the issue becomes problematic,<sup>63,78</sup> and the YTD system can be used to alleviate some of these limitations.

To prove the principle using the YTD, we first calculated the number of affibodies displayed per cell at different concentrations of aTc and as a function of the mean fluorescence of the displaying fraction of cells. Considering 0.5 million as the minimal number of cells and 0.05 mL as the minimum volume for the binding reaction, we compared the standard GAL-based yeast display and the YTD induced with 1, 5, 50, and 150 ng/mL aTc to assess the apparent  $K_D$ . As expected, fixing the volume did not work for the standard yeast display system, yielding a  $K_D = 23.98 \pm 1.873$  nM, which is 6.6-fold higher than the correct value ( $K_D = 3.65$  nM) and confirms the ligand

depletion effects. Conversely, when we induced the affibody in the YTD system at 1 and 5 ng/mL aTc and performed the immunoassay in 0.1 mL of fixed volume, we obtained fitted  $K_D$  values of  $K_{D,1} = 3.55 \pm 0.811$  and  $K_{D,5} = 4.12 \pm 0.564$  nM, respectively, which reflect the true value accurately. At 50 ng/mL aTc, we obtained  $K_{D,50} = 5.01 \pm 0.384$  and  $K_{D,150} = 5.57 \pm 0.415$  nM, which show that as the display level increases, the assays exhibit ligand depletion artifacts (Figure 4c). While the presented example of ligand depletion represents extreme conditions that must be avoided during experiment design with the GAL-based system, these YTD results demonstrate how lowering the avidity of the affibody molecules on the yeast well below what is achievable with GAL promoters allowed us to conduct these binding assays in low volumes while avoiding ligand depletion artifacts.

This demonstrated how the YTD offers controlled display of binding proteins at low copy numbers per cell, allowing accurate determination of equilibrium binding constants in low-volume samples (in this case, 50  $\mu$ L). Ligand depletion effects were avoided under working conditions that allow pelleting cells (minimum 500,000 cells per reaction) while keeping sample volumes low, thus saving effort, time, and reagents. After assessing the lowest non-depleting conditions, the binding curve of a high-affinity receptor can be generated easily using a microtiter plate. These data demonstrate how the YTD can be especially useful for characterizing ultra-high-affinity binding interactions (i.e., pM  $K_D$ ).

Production and handling of complex and/or precious antigens/ligands are a significant obstacle in synthetic biology and immunology research, and the ability to conserve these reagents is seen as an advantage. Particularly, insoluble antigens or inorganic and biodevice surfaces are of interest in affinity protein selection and screening.<sup>47,79–85</sup> We anticipate that the YTD can address challenges in this area by providing a tool for titrating multivalency and switching the stringency of affinity-based screening based on the number of displayed receptors on the yeast surface.

## CONCLUSIONS

Yeast surface display is a well-established platform for *in vitro* protein engineering and evolution. Multivalency or avidity control would be a useful addition to standard yeast display in many protein engineering projects. By placing the genomic Aga1p gene and the plasmid-borne fusion between Aga2p and the POI under transcriptional control by WTC<sub>846</sub>, we could demonstrate effective titration of the number of protein copies on the cell surface and the fraction of induced cells depending on the aTc inducer concentration. The YTD system modulates the maximum fraction of cells displaying the POI and the amount of displayed POI per cell (median fluorescence) over a wide range. Furthermore, the system reduced the induction time required for expression and display from 24 to 48 h for typical GAL-induction protocols down to  $\sim$ 5 h. The YTD system furthermore exhibited low variability and uniformity in the number of displayed constructs for the small collection of POIs that we tested.

We demonstrated that our system could be used to control phenotypic cell activity with three specific applications. First, we achieved fine discrimination of specific activity levels of displayed enzyme variants. Second, we showed the regulation of cell adhesion under shear stress through display copy number titration. Finally, we demonstrated improved quantification of receptor-ligand binding affinity in a low-volume

regime that avoided ligand depletion artifacts. We envision that the YTD system will find applications in various biomolecular engineering projects and address current limitations and bottlenecks in high-throughput screening based on yeast display.

## ASSOCIATED CONTENT

### Supporting Information

The Supporting Information is available free of charge at <https://pubs.acs.org/doi/10.1021/acssynbio.2c00351>.

Primers for strain engineering and cloning; strains used in this study; systems comparison and characterization of titrated enzymes; analysis of Gal induction of protein display; correlation of titrated cell adhesion to protein display and binding curves for ligand-depletion effect demonstration; and simulations of titrated antigen binding (PDF)

## AUTHOR INFORMATION

### Corresponding Author

Michael A. Nash – Department of Chemistry, University of Basel, Basel 4058, Switzerland; Swiss Nanoscience Institute, University of Basel, Basel 4056, Switzerland; Department of Biosystems Science and Engineering, ETH Zurich, Basel 4058, Switzerland; [orcid.org/0000-0003-3842-1567](https://orcid.org/0000-0003-3842-1567); Email: [michael.nash@unibas.ch](mailto:michael.nash@unibas.ch)

### Authors

Joanan Lopez-Morales – Department of Chemistry, University of Basel, Basel 4058, Switzerland; Swiss Nanoscience Institute, University of Basel, Basel 4056, Switzerland; Department of Biosystems Science and Engineering, ETH Zurich, Basel 4058, Switzerland  
Rosario Vanella – Department of Chemistry, University of Basel, Basel 4058, Switzerland; Department of Biosystems Science and Engineering, ETH Zurich, Basel 4058, Switzerland; [orcid.org/0000-0001-7503-1627](https://orcid.org/0000-0001-7503-1627)  
Gordana Kovacevic – Department of Chemistry, University of Basel, Basel 4058, Switzerland; Department of Biosystems Science and Engineering, ETH Zurich, Basel 4058, Switzerland  
Mariana Sá Santos – Department of Chemistry, University of Basel, Basel 4058, Switzerland; Department of Biosystems Science and Engineering, ETH Zurich, Basel 4058, Switzerland; [orcid.org/0000-0002-9227-7941](https://orcid.org/0000-0002-9227-7941)

Complete contact information is available at: <https://pubs.acs.org/doi/10.1021/acssynbio.2c00351>

### Author Contributions

J.L.-M.: conceptualization, methodology, investigation, formal analysis, writing—original draft, and visualization. R.V.: conceptualization, investigation (strain engineering), validation, and writing—review and editing. G.K.: investigation, validation, data curation, resources, and writing—review and editing. M.S.S.: investigation and formal analysis. M.A.N.: data curation, supervision, project administration, funding acquisition, and writing—review and editing.

### Notes

The authors declare no competing financial interest.

## ACKNOWLEDGMENTS

This work was supported by the University of Basel, the ETH Zurich, the Swiss Nanoscience Institute, the Mexican CONACYT program, the Swiss National Science Foundation (200021\_175478 and NCCR Molecular Systems Engineering), and an ERC Starting Grant (MMA 715207). We thank Fabian Rudolf and Asli Azizoglu for the plasmid starting materials and helpful discussions. We also thank Sai Reddy and Joseph Taft for useful discussions.

## REFERENCES

- (1) Boder, E. T.; Wittrup, K. D. Yeast Surface Display for Screening Combinatorial Polypeptides Libraries. *Nat. Biotechnol.* **1997**, *15*, 553–557.
- (2) Feldhaus, M.; Siegel, R. Flow Cytometric Screening of Yeast Surface Display Libraries. *Methods Mol. Biol.* **2004**, *263*, 311–332.
- (3) Angelini, A.; Chen, T. F.; de Picciotto, S.; Yang, N. J.; Tzeng, A.; Santos, M. S.; Van Deventer, J. A.; Traxlmayr, M. W.; Wittrup, K. D. Protein Engineering and Selection Using Yeast Surface Display. *Methods Mol. Biol.* **2015**, *1319*, 3–36.
- (4) Liu, B. *Yeast Surface Display: Methods, Protocols, and Applications*; Liu, B., Ed.; Humana Press, 2015.
- (5) Orcutt, K. D.; Wittrup, K. D. Yeast Display and Selections. In *Antibody Engineering*; Kontermann, R., Dübel, S., Eds.; Springer Berlin Heidelberg: Berlin, Heidelberg, 2010; pp 207–233.
- (6) Sun, Y.; Ban, B.; Bradbury, A.; Ansari, G. A. S.; Blake, D. A. Combining Yeast Display and Competitive FACS to Select Rare Hapten-Specific Clones from Recombinant Antibody Libraries. *Anal. Chem.* **2016**, *88*, 9181–9189.
- (7) Könnig, D.; Kolmar, H. Beyond Antibody Engineering: Directed Evolution of Alternative Binding Scaffolds and Enzymes Using Yeast Surface Display. *Microb. Cell Fact.* **2018**, *17*, 32.
- (8) Gebauer, M.; Skerra, A. Engineered Protein Scaffolds as Next-Generation Therapeutics. *Annu. Rev. Pharmacol. Toxicol.* **2020**, *60*, 391–415.
- (9) Müller, M. R.; O'Dwyer, R.; Kovaleva, M.; Rudkin, F.; Dooley, H.; Barelle, C. J. Generation and Isolation of Target-Specific Single-Domain Antibodies from Shark Immune Repertoires. *Methods Mol. Biol.* **2012**, *907*, 177–194.
- (10) Kruziki, M. A.; Bhatnagar, S.; Woldring, D. R.; Duong, V. T.; Hackel, B. J. A 45-Amino-Acid Scaffold Mined from the PDB for High-Affinity Ligand Engineering. *Chem. Biol.* **2015**, *22*, 946–956.
- (11) Zorniak, M.; Clark, P. A.; Umlauf, B. J.; Cho, Y.; Shusta, E. V.; Kuo, J. S. Yeast Display Biopanning Identifies Human Antibodies Targeting Glioblastoma Stem-like Cells. *Sci. Rep.* **2017**, *7*, 15840.
- (12) Jenson, J. M.; Xue, V.; Stretz, L.; Mandal, T.; Reich, L. L.; Keating, A. E. Peptide Design by Optimization on a Data-Parameterized Protein Interaction Landscape. *Proc. Natl. Acad. Sci. U.S.A.* **2018**, *115*, E10342–E10351.
- (13) Andres, F.; Schwill, M.; Boersma, Y. L.; Plückthun, A. High-Throughput Generation of Bispecific Binding Proteins by Sortase A-Mediated Coupling for Direct Functional Screening in Cell Culture. *Mol. Cancer Ther.* **2020**, *19*, 1080–1088.
- (14) Wang, E. Y.; Dai, Y.; Rosen, C. E.; Schmitt, M. M.; Dong, M. X.; Ferré, E. M. N.; Liu, F.; Yang, Y.; Gonzalez-Hernandez, J. A.; Meffre, E.; Hinchcliffe, M.; Koumpouras, F.; Lionakis, M. S.; Ring, A. M. REAP: A Platform to Identify Autoantibodies That Target the Human Exoproteome; bioRxiv, 2021, 202102.11.430703.
- (15) Scholler, N. Selection of Antibody Fragments by Yeast Display. *Methods Mol. Biol.* **2012**, *907*, 259–280.
- (16) Tillotson, B. J.; de Larrinoa, I. F.; Klavas, C. A.; Shusta, D. M.; Shusta, E. V. Antibody Affinity Maturation Using Yeast Display with Detergent-Solubilized Membrane Proteins as Antigen Sources. *Protein Eng. Des. Sel.* **2012**, *26*, 101–112.
- (17) Boder, E. T.; Raeeszadeh-Sarmazdeh, M.; Price, J. V. Engineering Antibodies by Yeast Display. *Arch. Biochem. Biophys.* **2012**, *526*, 99–106.
- (18) Blazic, M.; Kovacevic, G.; Prodanovic, O.; Ostafe, R.; Gavrovic-Jankulovic, M.; Fischer, R.; Prodanovic, R. Yeast Surface Display for the Expression, Purification and Characterization of Wild-Type and B11 Mutant Glucose Oxidases. *Protein Expr. Purif.* **2013**, *89*, 175–180.
- (19) Zhang, K.; Bhuripanyo, K.; Wang, Y.; Yin, J. Coupling Binding to Catalysis: Using Yeast Cell Surface Display to Select Enzymatic Activities. *Methods Mol. Biol.* **2015**, *1319*, 245–260.
- (20) Kovačević, G.; Ostafe, R.; Balaž, A. M.; Fischer, R.; Prodanović, R. Development of GFP-Based High-Throughput Screening System for Directed Evolution of Glucose Oxidase. *J. Biosci. Bioeng.* **2019**, *127*, 30–37.
- (21) Vanella, R.; Ta, D. T.; Nash, M. A. Enzyme-Mediated Hydrogel Encapsulation of Single Cells for High-Throughput Screening and Directed Evolution of Oxidoreductases. *Biotechnol. Bioeng.* **2019**, *116*, 1878–1886.
- (22) Traxlmayr, M. W.; Shusta, E. V. Directed Evolution of Protein Thermal Stability Using Yeast Surface Display. *Methods Mol. Biol.* **2017**, *1575*, 45–65.
- (23) Ostafe, R.; Prodanovic, R.; Nazor, J.; Fischer, R. Ultra-High-Throughput Screening Method for the Directed Evolution of Glucose Oxidase. *Chem. Biol.* **2014**, *21*, 414–421.
- (24) Tanaka, T.; Yamada, R.; Ogino, C.; Kondo, A. Recent Developments in Yeast Cell Surface Display toward Extended Applications in Biotechnology. *Appl. Microbiol. Biotechnol.* **2012**, *95*, 577–591.
- (25) Reich, L. L.; Dutta, S.; Keating, A. E. SORTCERY-A High-Throughput Method to Affinity Rank Peptide Ligands. *J. Mol. Biol.* **2015**, *427*, 2135–2150.
- (26) Gao, G.; Mao, R.-Q.; Xiao, Y.; Zhou, J.; Liu, Y.-H.; Li, G. Efficient Yeast Cell-Surface Display of an Endoglucanase of *Aspergillus flavus* and Functional Characterization of the Whole-Cell Enzyme. *World J. Microbiol. Biotechnol.* **2017**, *33*, 114.
- (27) Cherf, G. M.; Cochran, J. R. Applications of Yeast Surface Display for Protein Engineering. *Methods Mol. Biol.* **2015**, *1319*, 155–175.
- (28) Uchański, T.; Zögg, T.; Yin, J.; Yuan, D.; Wohlkönig, A.; Fischer, B.; Rosenbaum, D. M.; Kobilka, B. K.; Pardon, E.; Steyaert, J. An Improved Yeast Surface Display Platform for the Screening of Nanobody Immune Libraries. *Sci. Rep.* **2019**, *9*, 382.
- (29) Wang, X. X.; Shusta, E. V. The Use of scFv-Displaying Yeast in Mammalian Cell Surface Selections. *J. Immunol. Methods* **2005**, *304*, 30–42.
- (30) Hackel, B. J. Ligand Engineering Using Yeast Surface Display. *Methods Mol. Biol.* **2014**, *1163*, 257–271.
- (31) Kuroda, K.; Ueda, M. Generation of Arming Yeasts with Active Proteins and Peptides via Cell Surface Display System: Cell Surface Engineering, Bio-Arming Technology. *Methods Mol. Biol.* **2014**, *1152*, 137–155.
- (32) Younger, D.; Berger, S.; Baker, D.; Klavins, E. High-Throughput Characterization of Protein–protein Interactions by Reprogramming Yeast Mating. *Proc. Natl. Acad. Sci. U.S.A.* **2017**, *114*, 12166–12171.
- (33) Zhang, X.; Wang, J.; Wen, K.; Mou, Z.; Zou, L.; Che, X.; Ni, B.; Wu, Y. Antibody Binding Site Mapping of SARS-CoV Spike Protein Receptor-Binding Domain by a Combination of Yeast Surface Display and Phage Peptide Library Screening. *Viral Immunol.* **2009**, *22*, 407.
- (34) Greaney, A. J.; Loes, A. N.; Crawford, K. H. D.; Starr, T. N.; Malone, K. D.; Chu, H. Y.; Bloom, J. D. Comprehensive Mapping of Mutations in the SARS-CoV-2 Receptor-Binding Domain That Affect Recognition by Polyclonal Human Plasma Antibodies. *Cell Host Microbe* **2021**, *29*, 463–476.
- (35) Greaney, A. J.; Starr, T. N.; Gilchuk, P.; Zost, S. J.; Binshtein, E.; Loes, A. N.; Hilton, S. K.; Huddleston, J.; Eguia, R.; Crawford, K. H. D.; Dingens, A. S.; Nargi, R. S.; Sutton, R. E.; Suryadevara, N.; Rothlauf, P. W.; Liu, Z.; Whelan, S. P. J.; Carnahan, R. H.; Crowe, J. E., Jr.; Bloom, J. D. Complete Mapping of Mutations to the SARS-CoV-2 Spike Receptor-Binding Domain That Escape Antibody Recognition. *Cell Host Microbe* **2021**, *29*, 44–57.

- (36) Liang, Y.; Wan, Y.; Qiu, L.-W.; Zhou, J.; Ni, B.; Guo, B.; Zou, Q.; Zou, L.; Zhou, W.; Jia, Z.; Che, X.-Y.; Wu, Y. Comprehensive Antibody Epitope Mapping of the Nucleocapsid Protein of Severe Acute Respiratory Syndrome (SARS) Coronavirus: Insight into the Humoral Immunity of SARS. *Clin. Chem.* **2005**, *51*, 1382–1396.
- (37) Maute, R. L.; Gordon, S. R.; Mayer, A. T.; McCracken, M. N.; Natarajan, A.; Ring, N. G.; Kimura, R.; Tsai, J. M.; Manglik, A.; Kruse, A. C.; Gambhir, S. S.; Weissman, I. L.; Ring, A. M. Engineering High-Affinity PD-1 Variants for Optimized Immunotherapy and Immuno-PET Imaging. *Proc. Natl. Acad. Sci. U.S.A.* **2015**, *112*, E6506–E6514.
- (38) Rix, G.; Watkins-Dulaney, E. J.; Almhjell, P. J.; Boville, C. E.; Arnold, F. H.; Liu, C. C. Scalable Continuous Evolution for the Generation of Diverse Enzyme Variants Encompassing Promiscuous Activities. *Nat. Commun.* **2020**, *11*, 5644.
- (39) Wellner, A.; McMahon, C.; Gilman, M. S. A.; Clements, J. R.; Clark, S.; Nguyen, K. M.; Ho, M. H.; Shin, J.-E.; Feldman, J.; Hauser, B. M.; Caradonna, T. M.; Winkler, L. M.; Schmidt, A. G.; Marks, D. S.; Abraham, J.; Kruse, A. C.; Liu, C. C. *Rapid Generation of Potent Antibodies by Autonomous Hypermutation in Yeast*; bioRxiv, 2020.
- (40) Zahradnik, J.; Dey, D.; Marciano, S.; Schreiber, G. *An Enhanced Yeast Display Platform Demonstrates the Binding Plasticity under Various Selection Pressures*; bioRxiv, 2020, 202012.16.423176.
- (41) Golinski, A. W.; Mischler, K. M.; Laxminarayan, S.; Neurock, N. L.; Fossing, M.; Pichman, H.; Martiniani, S.; Hackel, B. J. High-Throughput Developability Assays Enable Library-Scale Identification of Producing Protein Scaffold Variants. *Proc. Natl. Acad. Sci. U.S.A.* **2021**, *118*, No. e2026658118.
- (42) Vincke, C.; Gutiérrez, C.; Wernery, U.; Devoogdt, N.; Hassanzadeh-Ghassabeh, G.; Muyldermans, S. Generation of Single Domain Antibody Fragments Derived from Camelids and Generation of Manifold Constructs. *Methods Mol. Biol.* **2012**, *907*, 145–176.
- (43) Teymenet-Ramírez, K. V.; Martínez-Morales, F.; Trejo-Hernández, M. R. Yeast Surface Display System: Strategies for Improvement and Biotechnological Applications. *Front. Bioeng. Biotechnol.* **2021**, *9*, 794742.
- (44) Kingsmore, S. F. Multiplexed Protein Measurement: Technologies and Applications of Protein and Antibody Arrays. *Nat. Rev. Drug Discovery* **2006**, *5*, 310–321.
- (45) Beck, M.; Schmidt, A.; Malmstroem, J.; Claassen, M.; Ori, A.; Szymborska, A.; Herzog, F.; Rinner, O.; Ellenberg, J.; Aebersold, R. The Quantitative Proteome of a Human Cell Line. *Mol. Syst. Biol.* **2011**, *7*, 549.
- (46) Campbell, R. M.; Dymshitz, J.; Eastwood, B. J.; Emkey, R.; Greenen, D. P.; Heering, J. M.; Johnson, D.; Large, T. H.; Littlejohn, T.; Montrose, C.; Nutter, S. E.; Sawyer, B. D.; Sigmund, S. K.; Smith, M.; Weidner, J. R.; Zink, R. W. *Data Standardization for Results Management*; Eli Lilly & Company, 2012.
- (47) Stern, L. A.; Csizmar, C. M.; Woldring, D. R.; Wagner, C. R.; Hackel, B. J. Titratable Avidity Reduction Enhances Affinity Discrimination in Mammalian Cellular Selections of Yeast-Displayed Ligands. *ACS Comb. Sci.* **2017**, *19*, 315–323.
- (48) McIsaac, R. S.; Gibney, P. A.; Chandran, S. S.; Benjamin, K. R.; Botstein, D. Synthetic Biology Tools for Programming Gene Expression without Nutritional Perturbations in *Saccharomyces Cerevisiae*. *Nucleic Acids Res.* **2014**, *42*, No. e48.
- (49) Kim, S. K.; Lee, D.-H.; Kim, O. C.; Kim, J. F.; Yoon, S. H. Tunable Control of an *Escherichia Coli* Expression System for the Overproduction of Membrane Proteins by Titrated Expression of a Mutant Lac Repressor. *ACS Synth. Biol.* **2017**, *6*, 1766–1773.
- (50) Pedone, E.; Postiglione, L.; Alicino, F.; Rocca, D. L.; Montes-Olivas, S.; Khazim, M.; di Bernardo, D.; Pia Cosma, M. P.; Marucci, L. A Tunable Dual-Input System for on-Demand Dynamic Gene Expression Regulation. *Nat. Commun.* **2019**, *10*, 4481.
- (51) Jost, M.; Santos, D. A.; Saunders, R. A.; Horlbeck, M. A.; Hawkins, J. S.; Scaria, S. M.; Norman, T. M.; Hussmann, J. A.; Liem, C. R.; Gross, C. A.; Weissman, J. S. *Titrating Gene Expression with Series of Systematically Compromised CRISPR Guide RNAs*; bioRxiv, 2019, 717389.
- (52) Bowman, E. K.; Deaner, M.; Cheng, J.-F.; Evans, R.; Oberortner, E.; Yoshikuni, Y.; Alper, H. S. Bidirectional Titration of Yeast Gene Expression Using a Pooled CRISPR Guide RNA Approach. *Proc. Natl. Acad. Sci. U.S.A.* **2020**, *117*, 18424–18430.
- (53) Arita, Y.; Kim, G.; Li, Z.; Friesen, H.; Turco, G.; Wang, R. Y.; Climie, D.; Usaj, M.; Hotz, M.; Stoops, E.; Baryshnikova, A.; Boone, C.; Botstein, D.; Andrews, B. J.; McIsaac, R. A *Genome-Scale Yeast Library with Inducible Expression of Individual Genes*; bioRxiv, 2020, 202012.30.424776.
- (54) Azizoglu, A.; Brent, R.; Rudolf, F. A Precisely Adjustable, Variation-Suppressed Eukaryotic Transcriptional Controller to Enable Genetic Discovery. *Elife* **2021**, *10*, No. e69549.
- (55) Schoeler, C.; Malinowska, K. H.; Bernardi, R. C.; Milles, L. F.; Jobst, M. A.; Durner, E.; Ott, W.; Fried, D. B.; Bayer, E. A.; Schulten, K.; Gaub, H. E.; Nash, M. A. Ultrastable Cellulose-Adhesion Complex Tightens under Load. *Nat. Commun.* **2014**, *5*, 5635.
- (56) Kovačević, G.; Ostafe, R.; Fischer, R.; Prodanović, R. Influence of Methionine Residue Position on Oxidative Stability of Glucose Oxidase from *Aspergillus Niger*. *Biochem. Eng. J.* **2019**, *146*, 143–149.
- (57) Daniel Gietz, R.; Woods, R. A. Transformation of Yeast by Lithium Acetate/single-Stranded Carrier DNA/polyethylene Glycol Method. In *Methods in Enzymology*; Guthrie, C., Fink, G. R., Eds.; Academic Press, 2002; Vol. 350, pp 87–96.
- (58) Keeseey, J. Biochemicals for Protein Research. In *Biochemical Information: A Revised Biochemical Reference Source*; Keeseey, J., Ed.; Boehringer Mannheim Biochemicals, 1987; Vol. 1, p 58.
- (59) Huo, Z.; Sá Santos, M.; Drenckhan, A.; Holland-Cunz, S.; Izbicki, J. R.; Nash, M. A.; Gros, S. J. Metastatic Esophageal Carcinoma Cells Exhibit Reduced Adhesion Strength and Enhanced Thermogenesis. *Cells* **2021**, *10*, 1213.
- (60) Santos, M. S.; Liu, H.; Schittny, V.; Vanella, R.; Nash, M. A. Correlating Single-Molecule Rupture Mechanics with Cell Population Adhesion by Yeast Display. *Biophys. Rep.* **2022**, *2*, 100035.
- (61) Boettiger, D. Quantitative Measurements of Integrin-Mediated Adhesion to Extracellular Matrix. *Methods in Enzymology*; Academic Press, 2007; Vol. 426, pp 1–25.
- (62) Boder, E. T.; Midelfort, K. S.; Wittrup, K. D. Directed Evolution of Antibody Fragments with Monovalent Femtomolar Antigen-Binding Affinity. *Proc. Natl. Acad. Sci. U.S.A.* **2000**, *97*, 10701–10705.
- (63) Chao, G.; Lau, W. L.; Hackel, B. J.; Sazinsky, S. L.; Lippow, S. M.; Wittrup, K. D. Isolating and Engineering Human Antibodies Using Yeast Surface Display. *Nat. Protoc.* **2006**, *1*, 755–768.
- (64) Swoboda, B. E.; Massey, V. Purification and properties of the glucose oxidase from *aspergillus niger*. *J. Biol. Chem.* **1965**, *240*, 2209–2215.
- (65) Vanella, R.; Bazin, A.; Ta, D. T.; Nash, M. A. Genetically Encoded Stimuli-Responsive Cytoprotective Hydrogel Capsules for Single Cells Provide Novel Genotype–Phenotype Linkage. *Chem. Mater.* **2019**, *31*, 1899–1907.
- (66) Liu, Z.; Liu, H.; Vera, A. M.; Bernardi, R. C.; Tinnefeld, P.; Nash, M. A. High Force Catch Bond Mechanism of Bacterial Adhesion in the Human Gut. *Nat. Commun.* **2020**, *11*, 4321.
- (67) Salama-Alber, O.; Jobby, M. K.; Chitayat, S.; Smith, S. P.; White, B. A.; Shimon, L. J. W.; Lamed, R.; Frolow, F.; Bayer, E. A. Atypical Cohesin-Dockerin Complex Responsible for Cell Surface Attachment of Cellulosomal Components: Binding Fidelity, Promiscuity, and Structural Buttresses. *J. Biol. Chem.* **2013**, *288*, 16827–16838.
- (68) Gallant, N. D.; García, A. J. Quantitative Analyses of Cell Adhesion Strength. *Methods Mol. Biol.* **2007**, *370*, 83–95.
- (69) Fuhrmann, A.; Engler, A. J. Acute Shear Stress Direction Dictates Adherent Cell Remodeling and Verifies Shear Profile of Spinning Disk Assays. *Phys. Biol.* **2015**, *12*, 016011.
- (70) Pascolutti, R.; Sun, X.; Kao, J.; Maute, R. L.; Ring, A. M.; Bowman, G. R.; Kruse, A. C. Structure and Dynamics of PD-L1 and an Ultra-High-Affinity PD-1 Receptor Mutant. *Structure* **2016**, *24*, 1719–1728.

- (71) Elin, W. E. G. New polypeptide having affinity to pd-ll. WO 2017072280 A1, April 5, 2017.
- (72) Goldstein, A.; Barrett, R. W. Ligand Dissociation Constants from Competition Binding Assays: Errors Associated with Ligand Depletion. *Mol. Pharmacol.* **1987**, *31*, 603–609.
- (73) VanAntwerp, J. J.; Wittrup, K. D. Fine Affinity Discrimination by Yeast Surface Display and Flow Cytometry. *Biotechnol. Prog.* **2000**, *16*, 31–37.
- (74) Carter, C. M. S.; Leighton-Davies, J. R.; Charlton, S. J. Miniaturized Receptor Binding Assays: Complications Arising from Ligand Depletion. *J. Biomol. Screen.* **2007**, *12*, 255–266.
- (75) Hulme, E. C.; Trevethick, M. A. Ligand Binding Assays at Equilibrium: Validation and Interpretation. *Br. J. Pharmacol.* **2010**, *161*, 1219–1237.
- (76) Gera, N.; Hussain, M.; Rao, B. M. Protein Selection Using Yeast Surface Display. *Methods* **2013**, *60*, 15–26.
- (77) Jarmoskaite, I.; AlSadhan, I.; Vaidyanathan, P. P.; Herschlag, D. How to Measure and Evaluate Binding Affinities. *Elife* **2020**, *9*, No. e57264.
- (78) Zajc, C. U.; Teufl, M.; Traxlmayr, M. W. Affinity and Stability/Stabilities Analysis of Yeast Displayed Proteins. In *Yeast Surface Display*; Traxlmayr, M. W., Ed.; Springer US: New York, NY, 2022; pp 155–173.
- (79) Silman, I. H.; Katchalski, E. Water-Insoluble Derivatives of Enzymes, Antigens, and Antibodies. *Annu. Rev. Biochem.* **1966**, *35*, 873–908.
- (80) Hattori, T.; Umetsu, M.; Nakanishi, T.; Togashi, T.; Yokoo, N.; Abe, H.; Ohara, S.; Adschiri, T.; Kumagai, I. High Affinity Anti-Inorganic Material Antibody Generation by Integrating Graft and Evolution Technologies: Potential of Antibodies as Biointerface Molecules. *J. Biol. Chem.* **2010**, *285*, 7784–7793.
- (81) Benatuil, L.; Perez, J. M.; Belk, J.; Hsieh, C.-M. An Improved Yeast Transformation Method for the Generation of Very Large Human Antibody Libraries. *Protein Eng. Des. Sel.* **2010**, *23*, 155–159.
- (82) Ebersbach, H.; Geisse, S. Antigen Generation and Display in Therapeutic Antibody Drug Discovery—a Neglected but Critical Player. *Biotechnol. J.* **2012**, *7*, 1433–1443.
- (83) Chimalakonda, A. P.; Yadav, R.; Marathe, P. Factors Influencing Magnitude and Duration of Target Inhibition Following Antibody Therapy: Implications in Drug Discovery and Development. *AAPS J.* **2013**, *15*, 717–727.
- (84) Kariolis, M. S.; Kapur, S.; Cochran, J. R. Beyond Antibodies: Using Biological Principles to Guide the Development of next-Generation Protein Therapeutics. *Curr. Opin. Biotechnol.* **2013**, *24*, 1072–1077.
- (85) Yang, Z.; Wan, Y.; Tao, P.; Qiang, M.; Dong, X.; Lin, C.-W.; Yang, G.; Zheng, T.; Lerner, R. A. A Cell-Cell Interaction Format for Selection of High-Affinity Antibodies to Membrane Proteins. *Proc. Natl. Acad. Sci. U.S.A.* **2019**, *116*, 14971–14978.